Quantifying Complexity in Quantum Phase Transitions
via Mutual Information Complex Networks

Marc Andrew Valdez, Daniel Jaschke, David L. Vargas, and Lincoln D. Carr

Department of Physics, Colorado School of Mines, Golden, Colorado 80401, USA

We quantify the emergent complexity of quantum states near quantum critical points on regular 1D lattices, via complex network measures based on quantum mutual information as the adjacency matrix, in direct analogy to quantifying the complexity of electroencephalogram or functional magnetic resonance imaging measurements of the brain. Using matrix product state methods, we show that network density, clustering, disparity, and Pearson's correlation obtain the critical point for both quantum Ising and Bose-Hubbard models to a high degree of accuracy in finite-size scaling for three classes of quantum phase transitions, Z_2, mean field superfluid to Mott insulator, and a Berzinskii-Kosterlitz-Thouless crossover.

Classical statistical physics has developed a powerful set of tools for analyzing complex systems, chief among them complex networks, in which connectivity and topology predominate over other system features [1]. Complex networks model systems as diverse as the brain and the internet; however, up until now they have been obtained in quantum systems by explicitly enforcing complex network structure in their quantum connections [2–7], e.g., entanglement percolation *on* a complex network [4]. In contrast, complexity measures on the brain observe emergent complexity arising *out of*, e.g., a regular array of EEG electrodes placed on the scalp, via an adjacency matrix formed from the classical mutual information calculated between them [8]. We apply the quantum generalization of this measure, an adjacency matrix of the quantum mutual information calculated on quantum states [9], to well-known quantum many-body models on regular 1D lattices, such as the Ising model, as sketched in Fig. 1, and uncover emergent quantum complexity that clearly identifies quantum critical points (QCPs) [10,11]. Quantum mutual information bounds two-point correlations from above [12], measurable in a precise and tunable fashion in, e.g., atom interferometry in 1D Bose gases [13], among many other quantum simulator architectures. Using matrix product state (MPS) computational methods [14–16], we demonstrate rapid finite size-scaling for both transverse Ising and Bose-Hubbard models, including Z_2, mean field, and Berzinskii-Kosterlitz-Thouless (BKT) quantum phase transitions.

As we move toward more and more complex quantum systems in materials design and quantum simulators, involving a hierarchy of scales, diverse interacting components, and a structured environment, we expect to observe long-lived dynamical features, fat-tailed distributions, and other key identifiers of complexity [17–19]. Such systems include quantum simulator technologies based on ultracold atoms and molecules [20], trapped ions [21], and Rydberg gases [22], as well as superconducting Josephson-junction

based nanoelectromechanical systems in which different quantum subsystems form compound quantum machines with both electrical and mechanical components [23]. A key area in which we have taken a first step beyond phase diagrams and ground state properties is nonequilibrium quantum dynamics, where critical exponents and renormalization group theory are only weakly applicable at best, e.g., in the Kibble-Zurek mechanism, and are hard to find any use for at all in far-from-equilibrium regimes. However, at the most basic level we can first ask, are quantum systems inherently complex? Must we impose complexity on quantum systems to obtain it [2–7], or is there a regime in which complexity naturally emerges, even in ground states of regular lattice models? In this Letter we show that emergent complexity can be well quantified in the simplest of 1D lattice quantum simulator models in terms of complexity measures around QCPs in direct analogy to similar measurements on the brain; moreover, we establish
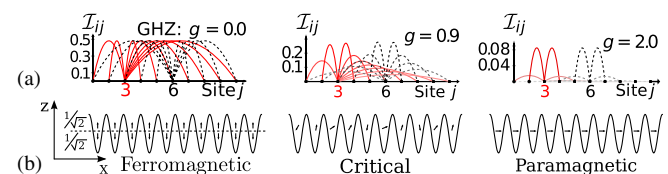

FIG. 1. Sketch of the mutual information complex network. A chain of L quantum bits for the transverse Ising model, the "fruit fly" of quantum many body physics. (a) Links originating from site 3 and site 6 for the mutual information complex network $\mathcal{I}_{ij}$, corresponding to phases and critical point in (b). In this weighted network, the height of the links in our sketch denotes their relative strength; note descending vertical axes from left to right. The entire complex network is far too dense to depict, so we show just two representative sites. (b) Sketch of ferromagnetic phase, critical point, and paramagnetic phase. The sinusoidal potential corresponds to an optical lattice for ultracold atoms or molecules. In the ferromagnetic limit the ground state is the Z_2 symmetric superposition between all spin up and all spin down, indicated by two rows of arrows.

a much-needed new set of tools for quantifying the complexity of far-from-equilibrium quantum dynamics.

Quantum phase transitions are often characterized by quantum averages over physical observables such as two-point correlators. For example, the transverse Ising model (TIM) consists of a chain of qubits with nearest neighbor z-z coupling J and a transverse field g. For large g, spins are not correlated in the z direction, while for small g the spins tend to align or antialign, depending on the sign of J. The quantum phase transition between large g (paramagnetic) and small g (ferro- or antiferromagnetic) at the QCP $g_c = 1$ is evidenced by a change in the long-range behavior of the two-point correlator $g_{ij}^{(2)} = \langle \hat{\sigma}_i^z \hat{\sigma}_j^z \rangle - \langle \hat{\sigma}_i^z \rangle \langle \hat{\sigma}_j^z \rangle$, where i, j are sites on a lattice and $\hat{\sigma}^z$ are measurements of spin in the z direction; alternate measures include the von Neumann entropy and concurrence [24]. The mutual information $\mathcal{I}_{ij}$ is bounded from below by $g_{ij}^{(2)}$, and indeed by any possible two-point correlator in the model [12]. In general, for quantum simulator technologies we obtain Hamiltonians for which we do not know *a priori* what the right correlator is or indeed if there is a quantum phase transition at all. Thus, mutual information provides a much more general tool to identify such quantum phase transitions than any particular physical correlator.

To establish the usefulness of mutual information complex networks, we consider both the TIM and the Bose-Hubbard model (BHM). The BHM balances particle tunneling J against on-site particle interaction U, with the filling factor controlled by the chemical potential μ; thus it has a richer phase diagram than the TIM, and exhibits both mean field transitions from Mott insulators to a superfluid phase as well as BKT crossovers at commensurate filling. We emphasize that both these models are studied heavily in quantum simulators experimentally and theoretically [20,21,25–27].

Quantum many-body Hamiltonians and mutual information.—The 1D TIM takes the form

$$\hat{H}_I = -J \sum_{i=1}^{L-1} \hat{\sigma}_i^z \hat{\sigma}_{i+1}^z - Jg \sum_{i=1}^{L} \hat{\sigma}_i^x, \qquad (1)$$

where $[\hat{\sigma}_j^\alpha, \hat{\sigma}_k^\beta] = 2i\delta_{jk}\epsilon_{\alpha\beta\gamma}\hat{\sigma}_k^\gamma$. The 1D BHM takes the form

$$\hat{H}_B = -J \sum_{i=1}^{L-1} (\hat{b}_i^\dagger \hat{b}_{i+1} + \text{H.c.}) + \frac{U}{2} \sum_{i=1}^{L} \hat{n}_i(\hat{n}_i - \mathbb{1}) - \mu \sum_{i=1}^{L} \hat{n}_i, \qquad (2)$$

where $[\hat{b}_i, \hat{b}_j^\dagger] = \delta_{ij}$ are bosonic annihilation and creation operators and $\hat{n}_i = \hat{b}_i^\dagger \hat{b}_i$. Both the TIM and BHM are standard workhorses of quantum many-body lattice physics [11]. The quantum mutual information $\mathcal{I}_{ij} \equiv \frac{1}{2}(S_i + S_j - S_{ij})$, with $\mathcal{I}_{ii} \equiv 0$, is constructed from the one and two point von Neumann entropies

$S_i = -\text{Tr}(\hat{\rho}_i \log_d \hat{\rho}_i)$, $S_{ij} = -\text{Tr}(\hat{\rho}_{ij} \log_d \hat{\rho}_{ij})$, with reduced density operators defined in terms of the partial trace as $\hat{\rho}_i = \text{Tr}_{k \neq i} \hat{\rho}$ and $\hat{\rho}_{ij} = \text{Tr}_{k \neq i,j} \hat{\rho}$. We take $d = 2$ for the TIM (qubits) and $d = n_{\max} + 1$ for the BHM, since particles can pile up on site in the latter, with $n_{\max} = 4$, a truncation parameter.

Complex network measures.—We use weighted generalizations of standard measures based on unweighted adjacency matrices [1]; a formal justification for and interpretation of this generalization procedure can be found in Ref. [28]. A primitive measure of a node's importance is the sum of the weights connecting it to other nodes in the network, $s_i \equiv \sum_{j=1}^{L} \mathcal{I}_{ij}$, where, s_i is called the strength of node i. The disparity Y_i of a node i in a network with L nodes is defined as a function over weighted connections to its neighbors,

$$Y_i \equiv \frac{1}{(s_i)^2} \sum_{j=1}^{L} (\mathcal{I}_{ij})^2 = \frac{\sum_{j=1}^{L} (\mathcal{I}_{ij})^2}{(\sum_{j=1}^{L} \mathcal{I}_{ij})^2}. \qquad (3)$$

Observe that if the mutual information between lattice sites adopts a constant value $\mathcal{I}_{ij} = a$, that $Y_i = a^2(L-1)/a^2(L-1)^2 = 1/(L-1)$, so that if a node has relatively uniform weights across its neighbors the disparity between nodes will be approximately $1/(L-1)$. On the other hand, if a particular $\mathcal{I}_{ij}$ takes on a dominant value b, then $Y_i \approx b^2/b^2 = 1$. The average disparity over all nodes in the network is $Y \equiv (1/L) \sum_{i=1}^{L} Y_i$. The clustering coefficient C is 3 times the ratio of triangles (three mutually connected vertices) to connected triples in an unweighted network. In our weighted network,

$$C \equiv \frac{\text{Tr}(\mathcal{I}^3)}{\sum_{j \neq i}^{L} \sum_{i=1}^{L} [\mathcal{I}^2]_{ij}}. \qquad (4)$$

The density D is the average fraction of the $\binom{L}{2}$ links that are present in the network:

$$D \equiv \frac{1}{L(L-1)} \sum_{i=1}^{L} s_i. \qquad (5)$$

As the number of nodes in an unweighted network is allowed to approach infinity a network is said to be *sparse* if $D \to 0$, and *dense* if $D > 0$ as the number of nodes in the network L approaches infinity [1]. Finally, a technique for assessing the similarity between two nodes i, j in a network is to compute the Pearson correlation coefficient between them,

$$r_{ij} \equiv \frac{\sum_{k=1}^{L} (\mathcal{I}_{ik} - \langle \mathcal{I}_i \rangle)(\mathcal{I}_{jk} - \langle \mathcal{I}_j \rangle)}{\sqrt{\sum_{k=1}^{L} (\mathcal{I}_{ik} - \langle \mathcal{I}_i \rangle)^2} \sqrt{\sum_{k=1}^{L} (\mathcal{I}_{jk} - \langle \mathcal{I}_j \rangle)^2}}, \qquad (6)$$

with $\langle \mathcal{I}_i \rangle$ the average of $\mathcal{I}_{ij}$ over j. r_{ij} is treating link weight as a random variable; the numerator of Eq. (6) is the

covariance of the weights of node i with the weights of node j, while the denominator is the standard deviation in the weights of node i multiplied by the standard deviation in the weights of node j. To restrict our study we focus on the Pearson correlation coefficient between the middle two sites of the lattice. These two nodes are spatially close to each other and far from boundaries, making them the most similar nodes in the network whose weights of connection are not strongly modified by boundary conditions; we thus choose $R \equiv r_{(L/2),(L/2)+1}$.

Numerical techniques.—We obtain our data with our widely used MPS open source code [16], a well-established algorithm [14]. The essence of the approach is data compression of a quantum many-body state onto a classical computer, using singular value decomposition. The key convergence parameter is the bond dimension χ, limiting the growth of spatial entanglement as defined by the truncated Schmidt number of the reduced density matrix [9]. We use bond dimensions of up to several hundred, which are adequate to establish the usefulness of our complex network measures to pin down QCPs, as is our aim (for extremely high accuracy calculations with bond dimensions in the thousands, see Ref. [29]). Our simulations are converged up to a variance tolerance of $10^{-10}(10^{-8})$ in the TIM (BHM). Mesoscopic corrections have been explored for the BHM in detail in our previous work [30].

Emergence of critical points.—Figure 2 shows a finite-size scaling study of complex network measures on the
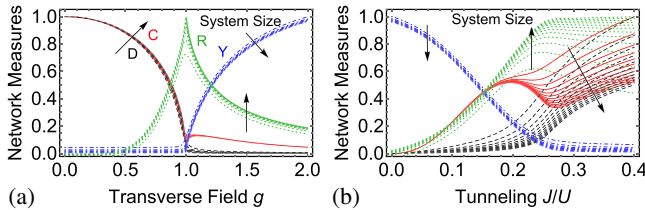

FIG. 2. Complex network measures on the mutual information. (a) Transverse quantum Ising model describing quantum spins (qubits). The clustering coefficient C and density D serve as order parameters for the ferromagnetic phase. The average disparity Y identifies the short range correlations of the paramagnetic ground state. The Pearson correlation coefficient R develops a cusp near the critical point $g_c = 1$, identifying a structured nature to correlations near criticality. (b) Bose-Hubbard model describing massive particles for commensurate lattice filling, with BKT crossover occurring in the limit $L \to \infty$ at a ratio of tunneling J to interaction U of $(J/U)_{BKT} = 0.305$; for smaller system sizes, the effective critical point [30] can be as small as $(J/U)_{BKT} \simeq 0.2$. The density and clustering coefficient grow as spatial correlations develop in the superfluid phase. The average disparity is high in the Mott insulator phase where correlations are short-ranged. Critical and crossover behavior is most evident in derivatives of these measures; see Fig. 3 and Table I. Note: all network measures have been self-normalized to unity for display on a single plot.

mutual information calculated with MPS code for these two models, for 1D lattices with ranges appropriate for experiments. Although we studied twelve network measures, we selected the four most relevant for brevity: density of links D, clustering coefficient C, average disparity Y, and Pearson correlation between middle lattice sites R; we also include other measures such as bond entropy S_B, negativity $\mathcal{N}$, correlation length ξ, and condensate depletion $\mathcal{D}$ for comparison purposes. All four network measures are clearly useful to identify phase transitions in the TIM and highlight different physical aspects. D is high in the TIM ferromagnetic and BHM superfluid phases where the nodes in the lattice are strongly connected, as sketched in Fig. 1(a). However, the quantum phase transition at the QCP is sharp at $L \to \infty$ for the TIM, where there is a Z_2 transition and $L \simeq 100$ suffices, whereas in the BHM we expect to observe a BKT crossover, which converges only for very large $L \simeq 1000$ [31], and is most apparent in the first and second derivative of D. The TIM paramagnetic and BHM Mott insulating phases are only sparsely connected. C follows a similar behavior except that for both the TIM and BHM it develops a local minimum near the QCP. This reflects the fact that the average number of connected triples is temporarily growing faster the control parameter (g for the TIM, J/U for the BHM) for the average number of triangles. Physically this could be because the length scale of correlations has become as long as one lattice spacing but not two, resulting in a period of rapid increase in mutual information between nearest neighbors relative to second nearest neighbors. In strong contrast to D and C, in the TIM ferromagnetic and BHM superfluid phases Y asymptotically approaches $(1/L - 1)$. In the TIM paramagnetic and BHM Mott insulating phases, where correlations decay exponentially, Y grows as spins become more tightly bound to their nearest neighbor relative to other qubits in the complex network. Finally, R has a completely different behavior, and clearly develops a cusp at the TIM QCP. Qualitatively, R is low in both the ferromagnetic and paramagnetic phases due to the relative homogeneity of correlations when $g \ll 1$ and when $g \gtrsim 2$. In contrast, near criticality the weights display an approximately linear relationship.

Finite-size scaling.—Figure 2(b) shows the BKT crossover transition for commensurate filling (average one particle per lattice site). However, a mean field phase transition at noncommensurate filling also appears in the BHM. As the Mott insulating phase is gapped (meaning the energy to create an excitation, even in the $L \to \infty$ limit, is nonzero), the usual way to find the boundaries of the Mott lobe (the region encompassing the Mott insulating phase) is to compute the energy required to add a particle or a hole to the insulator: the chemical potentials $\mu_c^p = E^p - E_0$ and $-\mu_c^h = E^h - E_0$, respectively [31]. Then one uses finite-size scaling to extrapolate μ_c^p and μ_c^h in L^{-1} to estimate the phase boundary. Instead of working with chemical
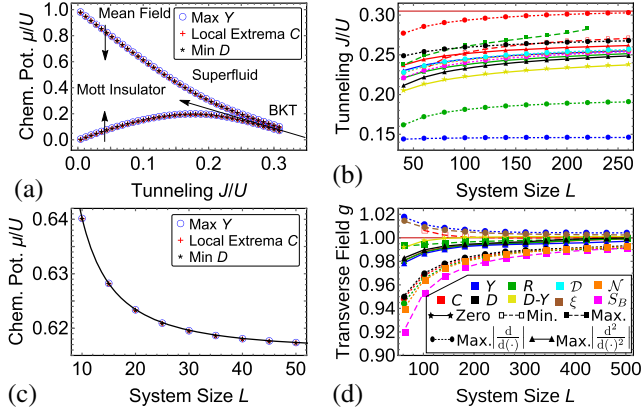
FIG. 3. Finite-size scaling for the Bose-Hubbard model and transverse Ising model. (a) BHM quantum phase diagram for fixed $L = 40$ showing superfluid and Mott Insulating phases with mean field phase transition along the Mott lobe and a BKT transition at its tip. (b) BHM BKT transition at unit filling. Scaling in $1/L$ places the critical point at $(J/U)_{BKT} = 0.314$ (clustering C, dashed red), 0.281 (average disparity Y, solid blue), and 0.289 (density D, black dashed), respectively. Compare to the best value to date [29,32] of 0.305, or the Luttinger liquid prediction of 0.328. (c) Approaching the BHM mean field superfluid to Mott insulator transition for fixed $(J/U) = 0.1$. Maximum disparity, central extrema in clustering, and minimum density scale towards the commensurate-incommensurate phase boundary and lie on top of each other. (d) Scaling of multiple measures and their derivatives for the TIM; see also Table I.

potentials, in Fig. 3(a) we use Y to obtain the first Mott lobe with both mean field and BKT crossover, shown here for $L = 40$. Figures 3(b) and 3(c) show finite size scaling in L towards the BKT crossover and the mean field phase transitions indicated in Fig. 3(a). Minimization of D and tracking the central extrema of C, which goes from a global minimum to a local maximum, result in similar estimates to Y. The BKT transition has been estimated by many methods in the past, including from the correlator $\langle \hat{b}_i^\dagger \hat{b}_{i+r} \rangle \sim r^{-K/2}$, taking advantage of the fact that at the QCP $K = 1/2$ [31], predicting $(J/U)_{BKT} = 0.29 \pm 0.01$; more recent results estimate $(J/U)_{BKT} = 0.305$ [29,32]. By fitting curves like those shown in Figs. 3(b) and 3(c) (BHM) and Fig. 3(d) (TIM), to power laws of the form $(J/U)_c(L) = (J/U)_c + AL^{-1/\nu'}$ (BHM) and $g_c(L) = g_c + AL^{-1/\nu}$ (TIM) we perform quantitative analysis of QCPs and provide errors due to the fitting procedure (see Supplemental Material [33] for a detailed explanation) in Table I. In particular, examining this data we observe that by measuring the complex network structure present in the quantum mutual information, we can estimate the QCP of the TIM to within 0.01% of its known value, that the Mott-insulator phase boundary can be reliably estimated by extremization of network quantities, and that the BKT transition at the tip of the Mott lobe, famously difficult to pin down without going to extremely large systems with thousands of sites with high accuracy, is estimated to within 5.3% using systems up to 260 sites via the max slope of D.

TABLE I. Quantitative finite-size scaling analysis of quantum critical points. Estimates for the critical point g_c and $(J/U)_{BKT}$ and scaling exponents ν, ν' for the transverse Ising and Bose Hubbard models, respectively, based on four complex network measures on the mutual information with standard quantum measures included for comparison. We include first and second derivatives (F.D., S.D.) since bare measures are often insufficient, an effect well known from one-point entanglement measures like the von Neumann entropy. We also note two other features: the local minimum in the clustering coefficient C (L.M.), and an intriguing point where normalized average disparity is equal to normalized density ($\tilde{Y} = \tilde{D}$). Entries are left blank when the measure fails to identify the critical point. Our complex network measures clearly perform as well or better than standard measures, particularly for the still improving estimates for the BHM BKT point [29].

Measure	g_c	ν	$(J/U)_{BKT}$	ν'
Density D F.D.	0.998 ± 0.005	0.962 ± 0.245	0.289 ± 0.067	2.980 ± 6.642
Density D S.D.	1.005 ± 0.011	1.549 ± 1.489	0.287 ± 0.055	2.706 ± 2.815
Disparity Y F.D.	1.003 ± 0.004	0.853 ± 0.618		
Disparity Y S.D.	0.999 ± 0.005	0.972 ± 0.597	0.281 ± 0.059	2.809 ± 4.529
Clustering C L.M.	1.000 ± 0.001	0.300 ± 0.393	0.281 ± 0.012	0.949 ± 0.471
Clustering C F.D.	0.997 ± 0.005	0.954 ± 0.237	0.314 ± 0.018	1.538 ± 1.343
Clustering C S.D.	1.003 ± 0.008	1.302 ± 1.013	0.281 ± 0.041	2.325 ± 3.172
Pearson R F.D.	0.998 ± 0.005	0.988 ± 0.232		
Pearson R S.D.	1.005 ± 0.012	1.517 ± 1.320	0.300 ± 0.111	3.842 ± 6.480
$\tilde{Y} = \tilde{D}$ L.M.	1.001 ± 0.002	0.539 ± 0.473	0.299 ± 0.148	4.441 ± 8.531
Bond Ent. S_B L.M.	1.000 ± 0.005	0.952 ± 0.146		
Bond Ent. S_B F.D.			0.283 ± 0.047	2.497 ± 2.714
Negativity $\mathcal{N}$ L.M.	1.000 ± 0.005	0.987 ± 0.207		
Negativity $\mathcal{N}$ F.D.			0.289 ± 0.069	3.030 ± 6.429
Corr. Len. ξ F.D.	1.001 ± 0.005	0.974 ± 0.888		
Depletion $\mathcal{D}$ F.D.			0.286 ± 0.054	2.680 ± 3.533

Conclusions.—We have shown that quantum complexity already emerges in a clearly quantifiable way in quantum states near quantum phase transitions in regular 1D lattices. In direct analogy to the complexity of electroencephalogram or functional magnetic resonance imaging measurements on the brain, our measures are built on taking the quantum mutual information as a weighted adjacency matrix, and reliably estimate quantum critical points for well-known quantum-many body models, in particular, the transverse Ising and Bose-Hubbard models. These models include three classes of phase transitions, Z_2, mean field superfluid to Mott insulator, and a BKT crossover; in each case we obtain rapidly converging accuracy for critical point values, a demonstrable improvement in finite-size scaling over all other known methods including, e.g., high order perturbation theory. To be specific, the improvements come from the fact that the complex network measures do not require *a priori* knowledge while retrieving important information about the quantum correlations. Our work sets the stage for application of a new set of quantum measures to quantify complexity of quantum systems where traditional correlation measures are at best weakly applicable. In future work we will apply our new methods to far-from-equilibrium dynamics in such systems, for instance, quantum cellular automata [18,19,34,35] and quantum degenerate ultracold molecules with a multiscale hierarchy of internal and external degrees of freedom [36].

[1] M. E. J. Newman, The structure and function of complex networks, SIAM Rev. **45**, 167 (2003).

[2] G. Bianconi and A.-L. Barabási, Bose-Einstein Condensation in Complex Networks, Phys. Rev. Lett. **86**, 5632 (2001).

[3] H. J. Kimble, The quantum internet, Nature (London) **453**, 1023 (2008).

[4] M. Cuquet and J. Calsamiglia, Entanglement Percolation in Quantum Complex Networks, Phys. Rev. Lett. **103**, 240503 (2009).

[5] S. Perseguers, M. Lewenstein, A. Acín, and J. I. Cirac, Quantum random networks, Nat. Phys. **6**, 539 (2010).

[6] G. Bianconi, Superconductor-insulator transition on annealed complex networks, Phys. Rev. E **85**, 061113 (2012).

[7] A. Halu, L. Ferretti, A. Vezzani, and G. Bianconi, Phase diagram of the Bose-Hubbard model on complex networks, Europhys. Lett. **99**, 18001 (2012).

[8] E. Bullmore and O. Sporns, Complex brain networks: graph theoretical analysis of structural and functional systems, Nat. Rev. Neurosci. **10**, 186 (2009).

[9] M. A. Nielsen and I. L. Chuang, *Quantum Computation and Quantum Information: 10th Anniversary Edition* (Cambridge University Press, New York, NY, 2011).

[10] *Understanding Quantum Phase Transitions*, edited by L. D. Carr (Taylor & Francis, Boca Raton, FL, 2010).

[11] S. Sachdev, *Quantum Phase Transitions* (Cambridge University Press, New York, 2011).

[12] M. M. Wolf, F. Verstraete, M. B. Hastings, and J. I. Cirac, Area laws in Quantum Systems: Mutual Information and Correlations, Phys. Rev. Lett. **100**, 070502 (2008).

[13] T. Langen, S. Erne, R. Geiger, B. Rauer, T. Schweigler, M. Kuhnert, W. Rohringer, I. E. Mazets, T. Gasenzer, and J. Schmiedmayer, Experimental observation of a generalized Gibbs ensemble, Science **348**, 207 (2015).

[14] U. Schollwoeck, The density-matrix renormalization group in the age of matrix product states, Ann. Phys. (Amsterdam) **326**, 96 (2011).

[15] D. Jaschke, M. L. Wall, and L. D. Carr, Open source Matrix Product States: Opening ways to simulate entangled many-body quantum systems in one dimension, arXiv: 1703.00387.

[16] Matrix product state open source code. http://sourceforge.net/projects/openmps/.

[17] *The National Academies Keck Futures Initiative: Complex Systems: Task Group Summaries* (National Academies Press, Washington, D.C., 2009).

[18] L. E. Hillberry, Master's thesis, Colorado School of Mines, 2016. http://inside.mines.edu/~lcarr/theses/hillberry_thesis_2016.pdf.

[19] D. L. Vargas, Master's thesis, Colorado School of Mines, 2016, http://inside.mines.edu/~lcarr/theses/vargas_thesis_2016.pdf.

[20] L. D. Carr, D. Demille, R. V. Krems, and J. Ye, Cold and ultracold molecules: Science, technology, and applications, New J. Phys. **11**, 055049 (2009).

[21] R. Blatt and C. F. Roos, Quantum simulations with trapped ions, Nat. Phys. **8**, 277 (2012).

[22] R. Loew, H. Weimer, J. Nipper, J. B. Balewski, B. Butscher, H. P. Buechler, and T. Pfau, An experimental and theoretical guide to strongly interacting Rydberg gases, J. Phys. B **45**, 113001 (2012).

[23] J. D. Teufel, T. Donner, Dale Li, J. W. Harlow, M. S. Allman, K. Cicak, A. J. Sirois, J. D. Whittaker, K. W. Lehnert, and R. W. Simmonds, Sideband cooling of micromechanical motion to the quantum ground state, Nature (London) **475**, 359 (2011).

[24] L. Amico, R. Fazio, A. Osterloh, and V. Vedral, Entanglement in many-body systems, Rev. Mod. Phys. **80**, 517 (2008).

[25] A. Lewenstein, M. Sanpera, V. Ahufinger, B. Damski, A. Sen De, and U. Sen, Ultracold atomic gases in optical lattices: Mimicking condensed matter physics and beyond, Adv. Phys. **56**, 243 (2007).

[26] J. W. Britton, B. C. Sawyer, A. C. Keith, C. C. Joseph Wang, J. K. Freericks, H. Uys, M. J. Biercuk, and J. J. Bollinger, Engineered two-dimensional Ising interactions in a trapped-ion quantum simulator with hundreds of spins, Nature (London) **484**, 489 (2012).

[27] B. Yan, S. A. Moses, B. Gadway, J. P. Covey, K. R. A. Hazzard, A. M. Rey, D. S. Jin, and J. Ye, Realizing a lattice spin model with polar molecules, Nature (London) **501**, 521 (2013).

[28] S. E. Ahnert, D. Garlaschelli, T. M. A. Fink, and G. Caldarelli, Ensemble approach to the analysis of weighted networks, Phys. Rev. E **76**, 016101 (2007).

[29] S. Ejima, H. Fehske, and F. Gebhard, Dynamic properties of the one-dimensional Bose-Hubbard model, Europhys. Lett. **93**, 30002 (2011).

[30] L. D. Carr, M. L. Wall, D. G. Schirmer, R. C. Brown, J. E. Williams, and Charles W. Clark, Mesoscopic effects in quantum phases of ultracold quantum gases in optical lattices, Phys. Rev. A **81**, 013613 (2010).

[31] T. D. Kühner, S. R. White, and H. Monien, One-dimensional Bose-Hubbard model with nearest-neighbor interaction, Phys. Rev. B **61**, 12474 (2000).

[32] J. Carrasquilla, S. R. Manmana, and M. Rigol, Scaling of the gap, fidelity susceptibility, and Bloch oscillations across the superfluid-to-Mott-insulator transition in the one-dimensional Bose-Hubbard model, Phys. Rev. A **87**, 043606 (2013).

[33] See Supplemental Material at http://link.aps.org/supplemental/10.1103/PhysRevLett.119.225301 for the comparison with established methods and measures, the computational scaling, and details of the error analysis.

[34] D. Bleh, T. Calarco, and S. Montangero, Quantum game of life, Europhys. Lett. **97**, 20012 (2012).

[35] P. Arrighi and J. Grattage, The quantum game of life, Phys. World **25**, 23 (2012).

[36] K. Maeda, M. L. Wall, and L. D. Carr, Hyperfine structure of the hydroxyl free radical (OH) in electric and magnetic fields, New J. Phys. **17**, 045014 (2015).